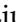




## Research Paper

# Rapid fluorescence imaging of spinal cord following epidural administration of a nerve-highlighting fluorophore

Wanguo Liu<sup>1</sup>, Rui Gu<sup>1</sup>, Qingsan Zhu<sup>1</sup>, Chunsheng Xiao<sup>2</sup>, Lanfeng Huang<sup>3</sup>, Xinming Zhuang<sup>4</sup>, Jingzhe Zhang<sup>1</sup>, Lidi Liu<sup>4</sup>, Ben Ma<sup>5</sup>, Huailin Yang<sup>2</sup>, Jianchao Ma<sup>1</sup>, Zhipeng Hu<sup>2</sup>, Chenglin Tang<sup>1</sup>, Shuhua Zhao<sup>6</sup>, Xuesi Chen<sup>2</sup>

1. Department of Orthopaedic Surgery, China-Japan Union Hospital, Jilin University, Changchun, China;
2. Key Laboratory of Polymer Ecomaterials, Changchun Institute of Applied Chemistry, Chinese Academy of Sciences, Changchun, China;
3. Department of Orthopaedic Surgery, The Second Hospital, Jilin University, Changchun, China;
4. Department of Orthopaedic Surgery, The First Hospital, Jilin University, Changchun, China;
5. Department of Orthopaedic Surgery, Jinhua Central Hospital, Zhejiang University, Jinhua, China;
6. Department of Occupational and Environmental Health, Public Health School, Jilin University, Changchun, China.

 Corresponding authors: zhuqs@jlu.edu.cn (Q. Zhu), xiaocs@ciac.ac.cn (C. Xiao), tcl6056@jlu.edu.cn (C. Tang), shzhao@jlu.edu.cn (S. Zhao)

© Ivyspring International Publisher. This is an open access article distributed under the terms of the Creative Commons Attribution (CC BY-NC) license (<https://creativecommons.org/licenses/by-nc/4.0/>). See <http://ivyspring.com/terms> for full terms and conditions.

Received: 2016.12.28; Accepted: 2017.03.02; Published: 2017.04.10

## Abstract

Iatrogenic spinal cord injury (SCI) is the most devastating complication of spine surgery, which usually results in permanent and serious disabilities of patients. Improvement of the visualization and discrimination of the spinal cord is critical for accuracy and safety during surgery; however, to date, there is no suitable technology to fulfill this clinical need. Here, we first show an efficient and rapid fluorescence imaging of the spinal cord in rabbit by epidural administration of a nerve-highlighting fluorophore, *i.e.* (*E, E*)-1,4-bis(*p*-aminostryl)-2-methoxy benzene (BMB). The BMB is firstly encapsulated into polymeric micelles to form a BMB-micelle (BMB-m) formulation with well-dispersion in normal saline solution. After epidural administration of BMB-m, BMB is transported by the flow of cerebrospinal fluid (CSF) and binds to the peripheral region of the white matter thus facilitating rapid staining of the spinal cord. Furthermore, this BMB imaging technology also holds great potential for visually monitoring the integrity of the spinal cord in real time and promptly identifying acute SCI during spine surgery.

Key words: fluorescence; image-guided surgery; spinal cord; epidural administration; cerebrospinal fluid; spinal cord injury.

## Introduction

The spinal cord, which is part of the central nervous system (CNS), is a pathway for conducting sensory and motor impulses between the brain and the peripheral nervous system [1, 2]. Iatrogenic spinal cord injury (SCI) is the most devastating complication of spine surgery with the incidence of approximately 0% to 2%, generally less than 1% [3-5]. The iatrogenic SCI usually results in chronic pain, loss of sensory and motor function, paralysis, and is even life-threatening [6, 7]. The spinal cord is soft, thin, fragile and lies deeply in narrow space, leading to increased

operation complexity and ultra-low fault tolerance during spine surgery [1, 2, 8]. Furthermore, the lack of clear anatomical landmarks is usually of a great challenge in the minimally invasive spinal surgery (MISS) due to the limited surgical and visual fields [9-11]. Thus, to improve intraoperative visualization and discrimination is of great importance for accuracy and safety of spine surgery.

Nowadays, a number of medical imaging technologies, including computed tomography (CT), magnetic resonance imaging (MRI) and positron

emission tomography (PET), have been widely used for accurately reflecting the anatomical structures and pathological changes in spinal cord [12-14]. However, these technologies are often applied in preoperative diagnosis and prognosis judgments, which can only offer limited help for improving the direct visualization of spinal cord by naked eye during surgery. Intraoperative electrophysiological monitoring (IOM) technologies, such as somatosensory evoked potentials (SEP), motor-evoked potentials (MEP) and electromyography (EMG), have also been developed for the assessment of the neurological integrity. However, false positive and negative reactions would occur as a result of anesthesia, hypothermia, improper operative position, etc. [15-17]. Moreover, all the IOM technologies still do not enable the direct observation and detection of the location and extent of SCI. Neuronal tracing technology based on the anterograde or retrograde axoplasmic transport of tracers in the neuronal tracts is another commonly used method for nerve labeling [18-20]. After local injection and tracing for a few days to several weeks, the nerve fibers can be visualized by immunohistochemistry, fluorescence microscopy or confocal laser scanning microscope (CLSM) [18-20]. However, the relatively slow tracing process and invasive manipulations make this technology impractical for clinical applications. Recent researches also demonstrated that the real-time fluorescent monitoring of cell structure, cellular activity and intercellular interactions can be readily achieved based on the expression of multi-color fluorescent proteins in nerve cells after genome editing [21-24]. However, even though this technology has been successfully applied in various animal models, the bio-safety of gene modified process is of significant concern before its clinical use.

To enhance the visualization of nerve tissue during surgery, a number of efforts have made to enhance the visualization of nerve tissue by systemic administration of a nerve-highlighting contrast agent [25-27]. For instance, Nguyen *et al.* developed a fluorescent peptide for specific highlight of peripheral nerves during surgery in mice. Unfortunately, due to the presence of the blood-brain barrier (BBB), this kind of fluorescent probe cannot enter the CNS (the brain and spinal cord) [25]. Gibbs-Strauss *et al.* also reported the imaging of dorsal root ganglia, trigeminal ganglia and intervertebral disk by intravenous administration of styryl pyridinium (FM) fluorophores. Similarly, these kinds of fluorescent agents did not highlight the CNS due to their large size [26].

Nevertheless, fluorescence-guided surgery (FGS) has become a promising technology for improving intraoperative visualization and accuracy [28-34]. Primary efforts have been devoted to guiding the resection of tumors in clinical practice [28-30]. However, to the best of our knowledge, this technology has not been used for spine surgery, which is probably due to the presence of BBB as discussed above. It is well-known that the epidural administration has been widely applied in clinical local anaesthesia and pain management with the benefits of fast acting in low dose, high drug targeting and less side effects [35-37]. Thus, in this paper, we propose an imaging method that rapidly visualizes spinal cord, making it possible to bring FGS into spine surgery and to reduce the risk of iatrogenic SCI, through epidural administration of a nerve-highlighting fluorophore. The (*E*, *E*)-1,4-bis(*p*-aminostyryl)-2-methoxy-benzene (BMB), a typical fluorophore that has been intensively reported for effective imaging of nerve tissues in mice, rats, pigs, baboons and even postmortem human, was synthesized and applied for this study [38-41]. The BMB was firstly encapsulated into polymeric micelles (BMB-m) and subsequently administrated by lumbar epidural injection for rapid and effective fluorescence imaging of spinal cord in rabbit. Furthermore, the possible mechanism for this ultra-bright imaging was investigated. Finally, the application of this imaging technology for detection of acute spinal cord injury was demonstrated.

## Materials and Methods

### Materials

The (*E*, *E*)-1,4-bis(*p*-aminostyryl)-2-methoxy-benzene (BMB) was synthesized according to the literature [38, 39]. Pluronic® F-127 and 3-(4,5-dimethyl-thiazol-2-yl)-2,5-diphenyl tetrazolium bromide (MTT) were purchased from Sigma-Aldrich (Shanghai, China). Purified deionized water was obtained from the Milli-Q Plus system. All chemicals were purchased from domestic reagent companies and used as received.

### Preparation and characterizations of BMB-m Formulation

The BMB was loaded into Pluronic® F-127 to form the BMB-m formulation. In brief, 50 mg of BMB and 500 mg of F-127 micelles were firstly dissolved in 5.0 mL of dimethyl sulfoxide (DMSO). The solution was then added dropwise into 50 mL of deionized water under magnetic stirring. The mixture was then transferred into the dialysis bag (MWCO 3500 Da) and dialyzed against deionized water for 24 h. After

that, the micellar solution was filtrated and subjected to lyophilization. The BMB-m was finally obtained as yellowish solid. The hydrodynamic radius ( $R_h$ ) of BMB-m was measured on a dynamic light scattering instrument (DLS, using Wyatt QELS™ plus Wyatt DAWN EOS, Wyatt Technology). The transmission electron microscopy (TEM) images of the BMB-m were recorded on a JEOL JEM-1011 transmission electron microscope. A drop of BMB-m suspension in deionized water ( $0.2 \text{ mg mL}^{-1}$ ) dropped on the 230 mesh copper grid coated with carbon and allowed to dry in air at room temperature before TEM measurements. The BMB content in BMB-m formulation was determined by a standard curve method on a PTI fluorescence spectroscope (Photon Technology International, U.S.A.).  $\lambda_{\text{ex}} = 400 \text{ nm}$  was applied for fluorescence measurements. The UV absorbance was recorded on a UV-2401PC spectrophotometer (Shimadzu, Japan).

### Cell Viability assays

The relative cytotoxicities of the BMB and BMB-m against L929 and PC-12 cells were evaluated in vitro by a standard MTT assay. The L929 and PC-12 cells were obtained from Cell Bank of Chinese of Academy of Science (Shanghai, China). Generally, the cells were seeded into 96-well plates (7000 cells/well) in  $180 \mu\text{L}$  of Dulbecco's modified Eagle medium (DMEM) with 10% fetal bovine serum, supplemented with  $50 \text{ U mL}^{-1}$  penicillin and  $50 \text{ U mL}^{-1}$  streptomycin, and then incubated at  $37 \text{ }^\circ\text{C}$  under 5%  $\text{CO}_2$  atmosphere for 24 h.  $20 \mu\text{L}$  of BMB suspensions (the BMB was firstly dissolved in DMSO and then diluted with DMEM to make the BMB suspensions with  $\text{DMSO} < 1 \text{ v/v\%}$  in DMEM) or BMB-m solutions in complete DMEM with different BMB concentrations ( $0\text{--}100.0 \text{ mg L}^{-1}$ ) were added to wells. The treated cells were cultured at  $37 \text{ }^\circ\text{C}$  for another 48 h. Then, MTT solution ( $5 \text{ mg/mL}$ ,  $20 \mu\text{L}$ ) was added into each well and the cells were incubated continually for another 4 h. The culture medium was withdrawn, and  $150 \mu\text{L}$  of DMSO was added into each well to dissolve the formazan. The absorbency of the solution was then measured on a Bio-Rad 680 microplate reader at  $490 \text{ nm}$ . Cell Viability (%) was calculated based on following equation:  $\text{Cell viability (\%)} = (A_{\text{sample}} / A_{\text{control}}) \times 100$ . Where  $A_{\text{sample}}$  and  $A_{\text{control}}$  represent the absorbency of the sample wells and control wells, respectively.

### Animals

Japanese white rabbits of either sex weighing roughly  $2.5 \text{ kg}$  were purchased from Hongda animal farms (Changchun, China). The experiments were conducted in accordance with the Guide for the Care

and Use of Laboratory Animals and approved by our Institutional Animal Investigation Committee (No: 2016-03-30) [42].

### Fluorescence Imaging System (FIS)

The fluorescence imaging system (FIS) contains the following principal components: a dark box module (length  $50 \text{ cm}$ , width  $32 \text{ cm}$ , and height  $32 \text{ cm}$ ), a  $365 \pm 25 \text{ nm}$  LED excitation light source with a power density of  $0.35 \text{ mW/cm}^2$  (Qinke Analysis Instrument Co., Shanghai, China), a  $550 \pm 25 \text{ nm}$  band pass emission filter (Xintianborui Light Electric Technology Co., Beijing, China), a color charged-coupled device (CCD) camera (YuanAO International Trade Co., Hongkong, China), and a computer control system with additional video centralized management software (Xiongmai Technology Co., Hangzhou, China). All fluorescent and white light images were acquired with  $20 \text{ ms}$  exposure time and identical normalizations. Fluorescence intensity was quantified using Image-Pro Plus 5.1 software (Media Cybernetics Inc., Silver Spring, MD, U.S.A.).

### BMB imaging of spinal cord *in vivo*

Prior to surgery, the lumbar area of animal was shaved, sterilized and then anesthetized by local infiltration using  $20 \text{ mL}$  of 1% lidocaine with 1:200,000 adrenaline. The paravertebral muscle was carefully detached away from the spinous process and laminar surface via the routine lumbar posterior approach through a midline  $4\text{-cm}$  incision. The ligamenta flava between the L6 and L7 laminae was then exposed after the partial removal of L7 spinous process. The rabbit was placed in the 30-degree elevated body position. After that, the BMB-m in normal saline solution was administrated using an L-shaped needle with a blunt tip ( $0.33 \text{ mm}$  outer diameter). The head part of the needle was firstly placed parallelly to the L7 laminae and subsequently caudally punctured into the yellow ligament to enter the epidural space with a sense of frustration. If the symptoms of neurological irritation occurred during epidural puncture, the subject was excluded from this study.

Firstly, each rabbit received a single epidural injection of  $0.2 \text{ mL}$  BMB-m solution at different BMB concentrations ranging from  $0.05$  to  $0.50 \text{ mg/mL}$  ( $n = 3$  rabbits per dose point). The rabbits were euthanized at  $30 \text{ min}$  post-injection. Rabbits given with a single injection of blank F127 micelles, normal saline ( $0.9\%$  sodium chloride solution) alone or untreated were used as the control. The spinal cord, sciatic nerve and surrounding tissues were then exposed and imaged in the FIS.

For the kinetics study, each rabbit received a single epidural injection of BMB-m solution (0.25 mg/mL  $\times$  0.2 mL, containing 50  $\mu$ g of BMB). The BMB-treated rabbits were euthanized at 0.25, 0.5, 1, 2, 4, 8, 14, and 24 h post-injection ( $n = 3$  rabbits per time point). The spinal cord, sciatic nerve and surrounding tissues were then exposed and imaged in the FIS.

### **BMB imaging of spinal cord via intravenous infusion**

BMB-m in normal saline solution (0.25 mg/mL  $\times$  20 mL, containing 5.0 mg of BMB) was intravenously infused via ear vein of rabbit ( $n=3$ ). At four hours post-injection [38, 40, 41], the rabbits were euthanized, and the spinal cord, sciatic nerve and surrounding tissues were then exposed and imaged in the FIS.

### **Dynamic viewing of the fluorescent imaging at T10 spinal cord after epidural administration of BMB-m at L6/7**

After exposure of ligamenta flava between the L6 and L7 laminae as described above, the soft tissues at around the T10 laminae were anesthetized by local infiltration using 20 mL of 1% lidocaine with 1:200,000 adrenaline, followed by the exposure of T10 spinal cord after the removal of the T10 spinous process and lamina via the routine thoracic posterior approach with a midline 4 cm incision. The fluorescence signal at the T10 segment was then dynamically monitored after L6/7 epidural administration of the BMB-m solution (0.25 mg/mL  $\times$  0.2 mL, containing 50  $\mu$ g of BMB) for 8 h.

### **Confocal laser scanning microscope (CLSM) observation of transverse section of spinal cord**

The BMB-stained spinal cord was collected and fixed with 4 wt% paraformaldehyde in PBS solution for 24 h. The typical spinal cords in the cervical, thoracic and lumbar segments were harvested, frozen with optimal cutting temperature compound and cut transversely into 20  $\mu$ m thick sections on a freezing microtome (Leica CM 1900). Then, the obtained spinal cord sections were covered by glass slips followed by addition of a drop of glycerol. After that, the images were measured under the CLSM (Zeiss LSM780).

### **Detection of spinal cord injury by BMB imaging**

The rabbit firstly received a single epidural injection of 0.2 mL of BMB-m in 0.9% sodium chloride solution (0.25 mg/mL, containing 50  $\mu$ g of BMB). In the meantime, the T10 spinal cord was exposed after the removal of spinous process and lamina via the routine thoracic posterior approach with a midline

4-cm incision. After that, the rabbit was further anesthetized by IV injection of 20 mg/kg sodium pentobarbital. At 30 min post-injection, the image of the T10 spinal cord was recorded in the FIS. Then, the T10 spinal cord was subjected to an acute injury induced either by Revilin method (clip compressive SCI model) [43] or Allen method (weight-drop SCI model) [44, 45]. For Revilin method, a clip crush injury was conducted on the dorsal half of the T10 spinal cord with ca. 50 g closing forces for one minute [43]. For Allen method, acute SCI was induced by dropping a constant weight (5 g) from a height of 30 cm (150 gram-centimeter force) onto the T10 spinal cord [44, 45]. The image at the T10 spinal cord was obtained immediately post-injury. After recording the fluorescent images, the spinal cord was harvested and fixed in 4 wt% paraformaldehyde in PBS solution for 24 h. The spinal cord at both the injury site and neighboring non-injury site was cut transversely on a freezing microtome (Leica CM 1900). Then, the obtained spinal cord sections were covered by glass slips followed by addition of a drop of glycerol. After that, the images were measured under the confocal laser scanning microscope (Zeiss LSM780).

### **Detection of BMB in CSF by RP-HPLC-ESI-MS**

The CSF was obtained from the cerebellomedullary cistern at 30 min post-injection of BMB-m solution. The sample was preserved at  $-20$  °C and then subjected to RP-HPLC-ESI-MS measurements. Electrospray ionization mass spectrometry (ESI-MS) was carried out on an electrospray ionization and quadrupole time-of-flight mass spectrometer (microTOF-Q II, Bruker Daltonics Inc., Germany) in positive ion mode. Reverse-phase high-performance liquid chromatography (RP-HPLC) was used for sample separation. A Zorbax Stablebond Analytical SB-C18 column (2.1  $\times$  50 mm, 1.8  $\mu$ m, Agilent Technologies) was used. The acetonitrile (ACN) was used as elution.

### **Statistical Analysis**

To assess the dose response of BMB on the fluorescence ratios of spinal cord to adipose (SC/A) at lumbar, thoracic and cervical spinal cord segments, two-way ANOVA with Bonferroni post-tests were performed. The staining thickness at the rim of spinal cord at different sections was analyzed using one-way ANOVA followed by Newman-Keuls Multiple Comparison Test. Data are expressed as the mean  $\pm$  SD. All statistical analysis was performed with GraphPad Prism (Prism, GraphPad, San Diego, CA). *P* value of less than 0.05 was considered statistically significant.

## Results

### Preparation and characterization of BMB loaded micelles

In this work, a typical nerve-highlighting fluorescent probe (BMB) was selected to test its potential for imaging of spinal cord. BMB is a Congo red derivative, which can bind specifically to myelin *in vivo* [38, 39]. Firstly, the BMB was encapsulated into the Pluronic® F-127 to improve aqueous solubility. The formed BMB-micelles (BMB-m) are of spherical structure with the size at *ca.* 84 nm (Figure 1A and B). In addition, the BMB-m is well-dispersed in normal saline to form clear solution at different BMB concentrations ranging from 0.05 to 0.5 mg/mL, which is ready for injection (Figure 1C). The BMB in DMSO shows typical UV absorbance and fluorescence emission with peaks at 398 and 500 nm, respectively (Figure 2B), while a broadening and blue-shifted UV absorbance with peak at 385 nm combined with a broadening and red-shifted fluorescence emission with peak at 525 nm were observed for BMB-m in normal saline solution (Figure 2C).

### In vivo imaging of spinal cord

Different doses of BMB (in BMB-m formulation) from 10 to 100  $\mu\text{g}/\text{rabbit}$  were epidurally administrated at the L6/7 level. After 30 min, the

spinal cord, sciatic nerves and surrounding tissues were exposed and imaged under the white light or UV light (365 nm). As shown in Figure 3A, there was almost no fluorescence in the spinal cord of control group. In contrast, green fluorescence staining of the spinal cord was clearly observed when administrated with BMB-m solution. The whole spinal cord was stained with BMB even at the dose as low as 10  $\mu\text{g}/\text{rabbit}$  and the fluorescence exhibited a decreasing gradient along with the lumbar, thoracic and cervical spinal cord segments. In the surrounding tissues, only the adipose tissue exhibited a visible auto-fluorescence. The auto-fluorescence of the adipose tissue was then used as the control to quantify the fluorescence intensity in the spinal cord. As illustrated in Figure 3B, the intensity of fluorescence increases as the dose of administrated BMB grows. The fluorescence ratios of spinal cord to adipose (SC/A) increase up to 7.8, 7.1 and 3.7 for lumbar, thoracic and cervical spinal cord segments, respectively, when 50  $\mu\text{g}/\text{rabbit}$  of BMB was applied. Further increasing the BMB dose to 100  $\mu\text{g}/\text{rabbit}$  resulted in little improvement of fluorescence intensity as compared with the group injected with BMB at the dose of 50  $\mu\text{g}/\text{rabbit}$  dose. Therefore, a single-dose of epidural BMB at 50  $\mu\text{g}/\text{rabbit}$  would be used for the following tests.

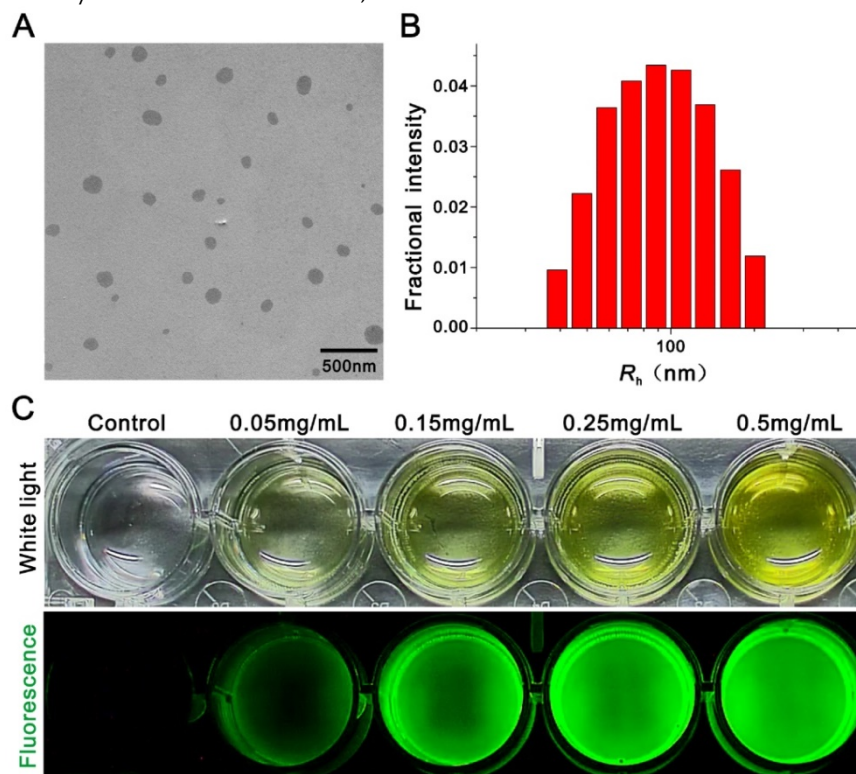


**Figure 1.** Preparation and characterization of BMB loaded micelles (BMB-m). (A) Transmission electron microscopy (TEM) image of BMB-m. (B) Dynamic light scattering (DLS) measurement of BMB-m in normal saline solution (0.1 mg/mL). (C) White light and fluorescence images of BMB-m in normal saline solution at different BMB concentrations.

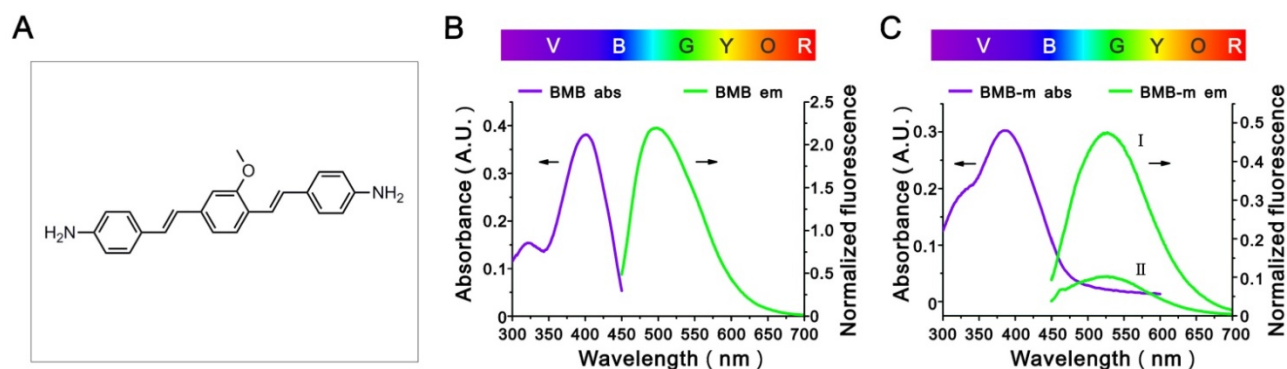


**Figure 2.** (A) The chemical structure of BMB. (B) The UV absorbance and fluorescence emission spectra of BMB. BMB was dissolved in DMSO at a concentration of 0.1 mg/mL for UV absorbance detection and a concentration of  $2 \times 10^{-4}$  mg/mL for fluorescence emission measurements. (C) The UV absorbance and fluorescence emission spectra of BMB-m. BMB-m was dispersed in normal saline at a concentration of 0.1 mg/mL for UV absorbance detection and concentrations of  $2 \times 10^{-3}$  mg/mL (I) and  $2 \times 10^{-4}$  mg/mL (II) for fluorescence emission measurements.

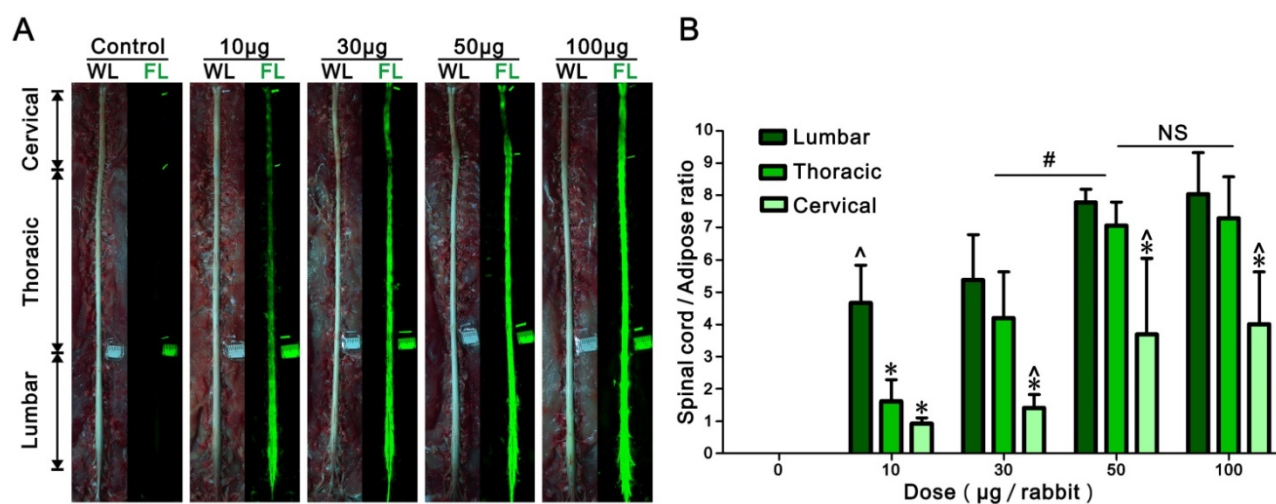


**Figure 3.** Dose response of BMB imaging of spinal cord at 30 min post-injection. (A) Observation of the spinal cord under white or UV light after epidural administration of BMB-m solution at different BMB doses (from 10 to 100 µg/rabbit). The complete imaging of spinal cord can be realized even at the dose as low as 10 µg/rabbit. (B) The fluorescence ratios of spinal cord to adipose (SC/A) at lumbar, thoracic and cervical spinal cord segments at different doses. The SC/A ratios of 50 µg/rabbit dose group are significantly higher than those of 10 µg/rabbit and 30 µg/rabbit dose groups ( $\#P < 0.05$ ), while it shows no remarkable difference with 100 µg/rabbit dose group. In the dose group of 10 µg/rabbit, the SC/A ratio of lumbar segment is significantly higher than those of thoracic and cervical segments ( $*P < 0.05$ ). In the dose groups from 30 to 100 µg/rabbit, the SC/A ratios of lumbar and thoracic segments are significantly higher than that of cervical segment ( $\wedge P < 0.05$ ). Data shown represent mean  $\pm$  SD of at least three experiments;  $\#P < 0.05$  versus 50 µg/rabbit dose group (two-way ANOVA with Bonferroni post-tests);  $*P < 0.05$  versus lumbar in same group (two-way ANOVA with Bonferroni post-tests);  $\wedge P < 0.05$  versus thoracic in same group (two-way ANOVA with Bonferroni post-tests); NS, not significant (two-way ANOVA with Bonferroni post-tests). WL: white light; FL: fluorescence.

The contrast imaging of spinal cord was then investigated at different time intervals after a single-dose epidural administration of BMB-m solution (containing 50 µg of BMB). As shown in **Figure S1 A**, the staining of the whole spinal cord occurred quickly at a very short time (<15 min). The brightest fluorescent imaging appeared at 30 min post-injection. After 30 min, the fluorescence on spinal cord would decrease over time and almost disappeared at 24 h, indicating that the BMB could be gradually metabolized from the spinal cord. Meanwhile, the meaningful imaging (SC/A ratio > 2) of lumbar, thoracic and cervical could last up to 14, 8 and 2 hours, respectively, which is sufficient for almost all spine surgeries (**Figure S1 B**).

To demonstrate the advantages of epidural administration of BMB for imaging of spinal cord, a comparative study was conducted by injecting 5.0 mg of BMB (in BMB-m formulation) into the rabbit via the ear vein. At 4 h post-injection [38, 40, 41], the fluorescence on different organs and tissues was obtained. Compared with the single-dose epidural administration of BMB-m solution (50 µg of BMB/rabbit), the intravenous injection group (5.0 mg of BMB/rabbit, which is 100-fold higher than that of the epidural administration group) exhibited relatively weak fluorescence in the spinal cord (0.17 fold) and enhanced fluorescence in the adipose tissue (3.8 fold) (**Figures S2 and S3**). In other words, the SC/A ratio of spinal cord in the epidural

administration group (6.7) is 19.1-fold higher than that in the intravenous administration group (0.35). Furthermore, the fluorescence signals also appeared in the sciatic nerve, muscle, liver, kidney, lung, etc. in the intravenous administration group, while none of these tissues/organs were detected with visible fluorescence in the epidural administration group (Figure S4).

### Mechanism study of BMB imaging of spinal cord *in vivo*

Based on the observations of rapid staining of the spinal cord, and the fluorescence signal ended at the dorsal root ganglion (Figure S5), we assumed that the BMB should be transported following the flow of cerebrospinal fluid (CSF). To validate this, an experiment was designed by dynamic viewing of the fluorescence imaging at the T10 spinal cord after administration of BMB-m solution (containing 50  $\mu\text{g}$  of BMB) at L6/7. As shown in Figure 4 and Video S1, there was no fluorescence at the T10 spinal cord in the first 2.5 minutes. After that, the BMB fluorescence became visible at the caudal site of T10 spinal cord and flowed quickly toward the cranial site. Several seconds later, the exposed window at T10 spinal cord was completely filled with BMB fluorescence, and the

fluorescence intensity would become stronger along with the time passing. Similarly to the results showed in Figure S1, the strongest fluorescence appeared at around 30 min, after which the fluorescence intensity declined gradually. At the end of observation, a weak fluorescence was still visible at the T10 spinal cord, indicating that the useful fluorescence imaging could last up to 8 hours. The staining of spinal cord based on the CSF transporting from caudal to cranial site was further confirmed by CLSM observations (Figure S6). If the BMB is delivered by CSF from the caudal spinal cord to the cranial site, it could bind to the peripheral white matter of spinal cord in a pattern of decreasing concentration gradient. As observed by the CLSM (Figure S6), the fluorescence intensity and staining thickness at the rim of spinal cord decreased from lumbar section to cervical section. Therefore, it can be concluded that the BMB was first transferred across the dura, entering into the subarachnoid space and subsequently traveled with the CSF flow to stain the whole spinal cord rapidly (Figure 5). Moreover, the gradual decline of BMB fluorescence with the passing of time indicated that the BMB could be metabolized in spinal cord, which may be associated with the circulation and adsorption of CSF [46-49].

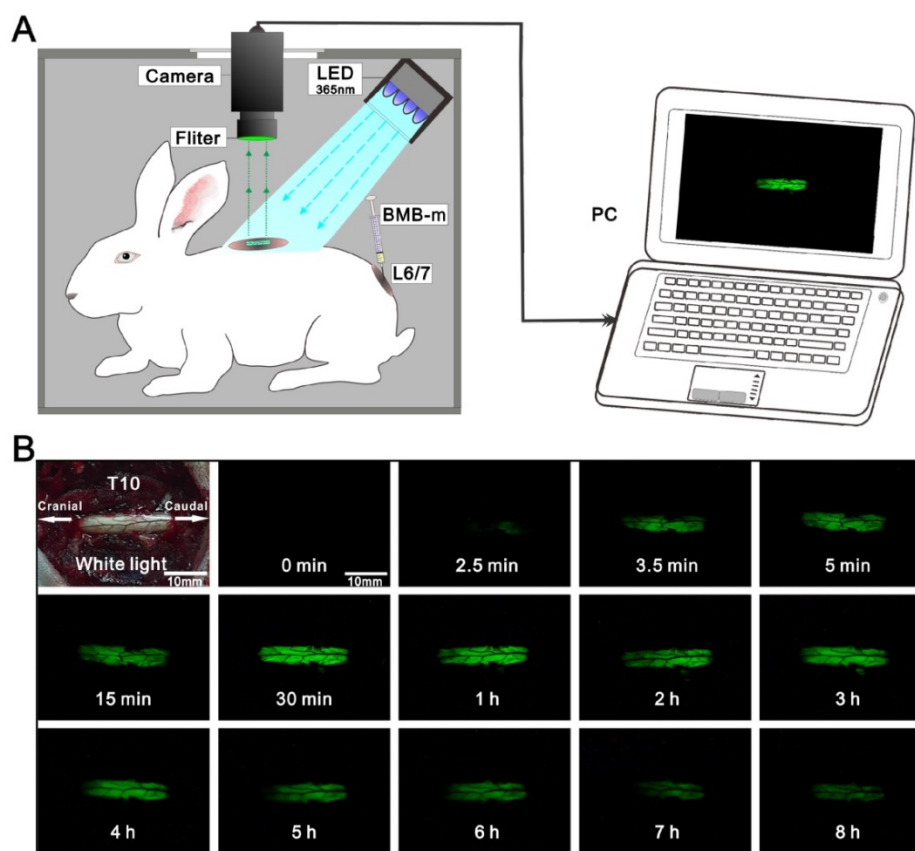


**Figure 4.** Dynamic viewing of the fluorescence at the T10 spinal cord in the rabbit (See Video S1). **(A)** Schematic illustration of real-time and in-situ monitoring of the fluorescence at the T10 spinal cord after a single-dose of epidural BMB (50  $\mu\text{g}$ , in BMB-m formulation) at L6/7. **(B)** The represent fluorescence images of the T10 spinal cord at different time points.

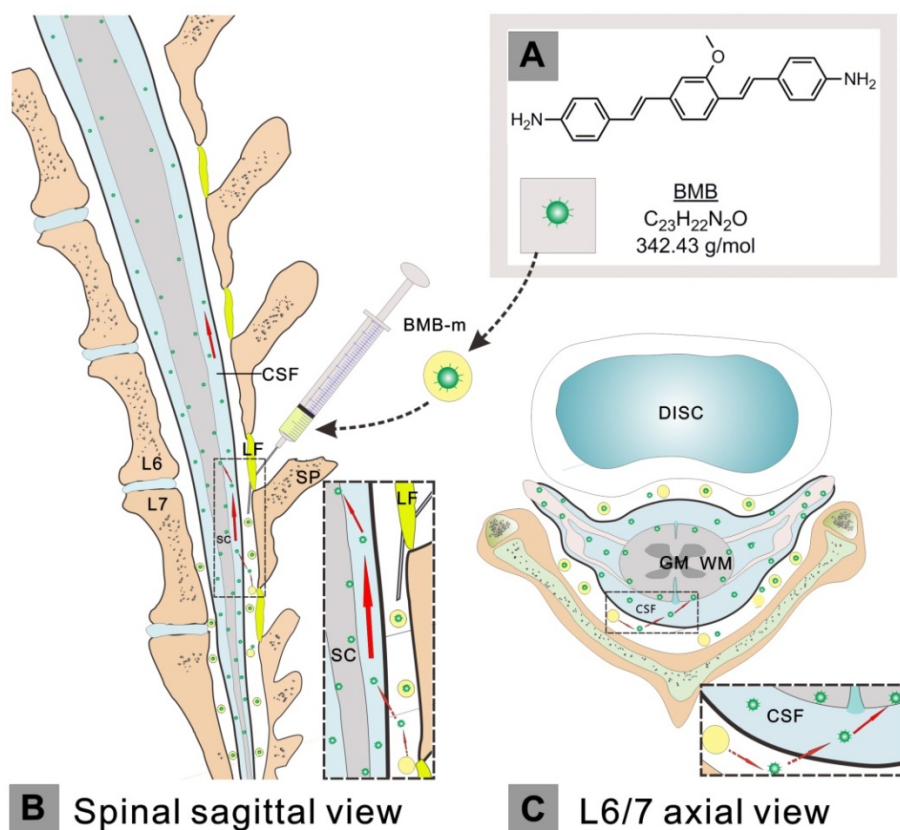


**Figure 5.** Schematic illustration of the administration, transportation and imaging behavior of BMB. The hydrophobic BMB (**A**) was firstly encapsulated in the amphiphilic block copolymer to form a BMB micellar formulation (BMB-m), which was well-dispersed in normal solution and ready for injection. The BMB-m was epidurally administrated at the L6/7 level (**B** and **C**). Upon injection, the BMB was conceived to pass across the dura and subsequently enter into the subarachnoid space filled with cerebrospinal fluid (CSF) (**B** and **C**, indicated by red dashed arrows). After that, the BMB could be transported by the flow of CSF in a direction from caudal spinal cord (SC) to the cranial site (**B**, indicated by large red solid arrows) and, meanwhile, bound to the peripheral white matter (WM) of spinal cord (**B** and **C**, indicated by small red solid arrows). GM: grey matter; LF: ligamentum flavum; SP: spinous process.

### Detection of iatrogenic spinal cord injury (SCI) by BMB imaging

In view of the rapid imaging of spinal cord by BMB, the potential application of this technology in detection of iatrogenic SCI was further investigated. The rabbits were pretreated by epidural administration of BMB-m solution (containing 50  $\mu\text{g}$  of BMB) at L6/7. At 30 min post-injection, two typical models, *i.e.* clip compressive SCI model (Rivlin method) [43] and weight-drop SCI model (Allen method) [44, 45], were established in situ to mimic the acute SCI during spine surgery (**Figure 6A** and **Figure 7A**). For both cases, the fluorescence at the T10 spinal cord was homogeneously distributed before the injury, while darkened fluorescence could be clearly observed on the injury sites (**Figure 6B–G** and **Figure 7B–G**). The diminished fluorescence is likely ascribed to the subdural hematoma and change of anatomy in white matter of spinal cord. Therefore, the experiment indicated that BMB imaging has tremendous potential in detection of acute SCI during surgery.

### Discussion

It is well-known that there are three protective membranes in the spinal meninges, including dura mater, arachnoid mater and pia mater [50, 51]. The space between arachnoid mater and pia mater is called subarachnoid space, which is filled with CSF [50, 51]. The arachnoid mater is the main permeability barrier for the macromolecules to enter the spinal cord [52–54]. However, it is relatively easy for small and lipophilic molecules to diffuse through the spinal meninges [52, 55, 56]. Based on this mechanism, some drugs with membrane penetrability have been widely applied in clinical anaesthesia and pain control via epidural injection [35–37]. In the present work, BMB is lipophilic with a molecular weight of 342 g/mol, which is similar to Bupivacaine (a representative lipophilic drug for epidural anaesthesia) [47,56]. Thus, it is anticipated that the BMB may be able to penetrate the spinal meninges. As a result, the rapid imaging of the whole spinal cord after epidural administration strongly suggested that the BMB molecule is penetrable towards the spinal meninges although the exact mechanism is not yet clear.



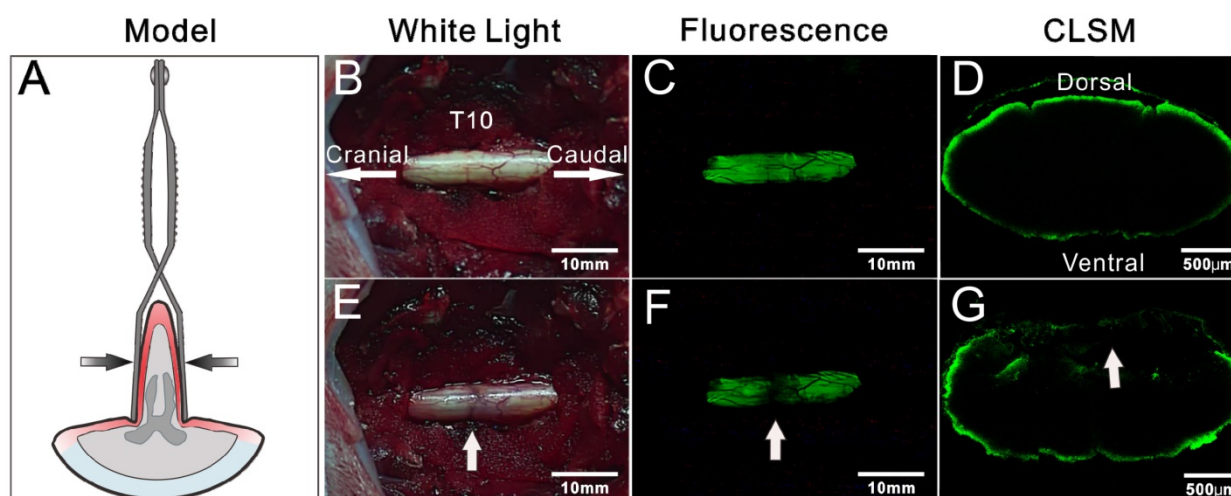


**Figure 6.** Detection of iatrogenic spinal cord injury by BMB imaging. **(A)** Schematic illustration of Rivlin method. **(B)** and **(E)** showing the in situ images of T10 spinal cord under white light before and after acute injury. **(C)** and **(F)** showing the in situ images of T10 spinal cord under UV light before and after acute injury. **(G)** and **(D)** showing the confocal laser scanning microscope (CLSM) images of transverse sections of spinal cord at the injury site and neighboring non-injury site, respectively.

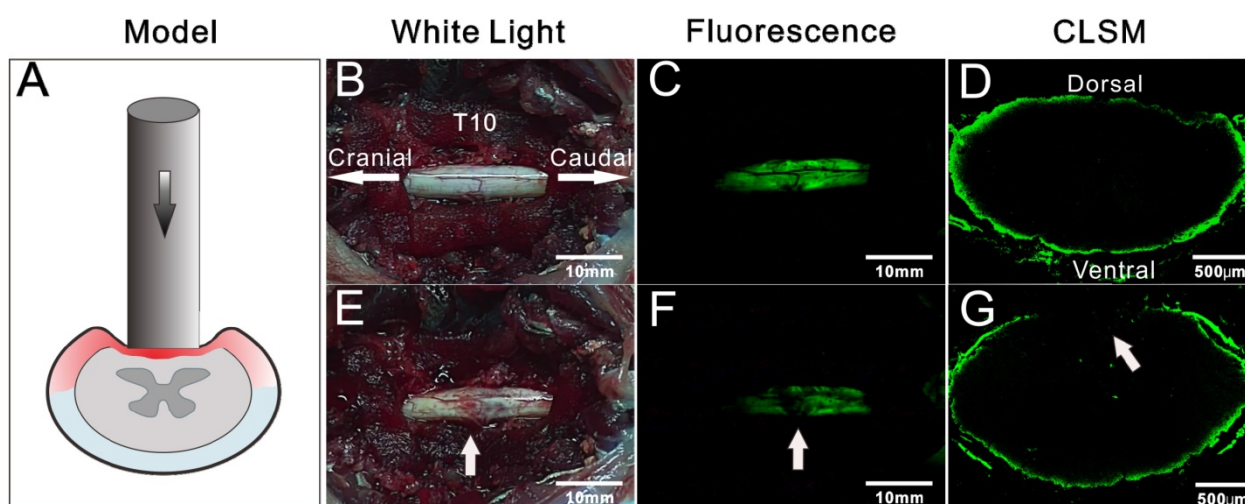


**Figure 7.** Detection of spinal cord injury by BMB imaging. **(A)** Schematic illustration of Allen method. **(B)** and **(E)** showing the in situ images of T10 spinal cord under white light before and after acute injury. **(C)** and **(F)** showing the in situ images of T10 spinal cord under UV light before and after acute injury. **(G)** and **(D)** showing the confocal laser scanning microscope (CLSM) images of transverse section of spinal cord at the injury site and neighboring non-injury site, respectively.

Besides the rapid imaging of spinal cord by BMB, it is also found that the fluorescence is ended at the dorsal root ganglion (Figure S5). Both of these observations have led to speculation that the CSF plays an important role in rapid transportation of the BMB. However, the behavior of CSF is still unclear due to the lack of effective tools to monitor the complex flow of CSF. For example, Di Chio *et al.* suggested a two-directional circulation flow in the spinal canal, *i.e.* downwardly directed in the posterior compartment and upwardly directed in the anterior compartment, based on the observation of transportation of radionuclides tracer in intraspinal space [57, 58]. But in another report by Greitz *et al.*, a pulsatile flow of CSF caused by the afflux of newly produced CSF from the ventricular system into

existing CSF was proposed [59]. Additionally, a bi-directional systolic-diastolic to-and-fro cranio-spinal CSF flow pattern associated with cardiac cycle was suggested [60]. In this study, we demonstrated, for the first time, a method that enables naked-eye observation of CSF fast-flowing from caudal to cranial site on the dorsal part of spinal cord following lumbar epidural administration of BMB-m in rabbit. Furthermore, the BMB was detectable in the CSF obtained from the cerebellomedullary cistern (Figure S7). These observations can not only confirm that the BMB is transported by the flow of CSF to realize rapid and efficient imaging of spinal cord, but also provide a valid tool for visual monitoring the flow of CSF.

In addition to the rapid labeling of spinal cord,

this technology has another advantage in using low-dose epidural BMB for the effective fluorescence imaging. Usually, for most of the nerve-highlighting agents, it is hard to label the nerve tissues in the CNS via intravenous injection due to the impermeability against the BBB [25-27, 41]. Also, these agents have some conspicuous drawbacks such as larger dose, time-consuming and large accumulation in non-nerve tissues when administered intravenously [27, 40, 41]. Inspired by the clinical epidural anesthesia, the BMB in micellar formulation was administered via the epidural route. As a result, the epidural administration group given a lower dose of BMB (100-fold less than the intravenous administration group) demonstrated a significantly higher SC/A as compared with the intravenous administration group. Moreover, large accumulation of BMB in non-nerve tissues were clearly observed in the intravenous administration group, while no fluorescence could be detected in these non-nerve tissues in the epidural administration group. In summary, this work has demonstrated, for the first time, the rapid and effective imaging of spinal cord by epidural administration of a low-dose fluorescence probe, which can avoid the BBB encountered by intravenous administration and thus provides a new path for CNS imaging.

In spine surgery, any incidents during decompression, fixation or correction may lead to acute SCI and further induce serious complications [3-5]. In particular, the spinal cord and nerve roots are usually placed at risk for direct trauma due to the limited surgical field and anatomical discrimination when small incisions are applied [9-11]. Currently, IOM technologies are the most popular methods for intraoperatively monitoring the integrity of neurological function [15-17]. However, they fail to meet the requirements for the direct observation and detection of the location and extent of SCI. In this work, we have demonstrated that the BMB staining of spinal cord occurred in the peripheral region of the white matter, but not the whole cross-section of spinal cord. In this case, any structural changes of the white matter or subdural hematoma in acute SCI would be indicated by the pattern of BMB fluorescence. To test it, two kinds of SCI models were established and the results revealed that significantly reduced fluorescent signals of spinal cord were observed in both SCI models. As shown in **Figures 6** and **7**, both subdural hematoma (**Figures 6E** and **7E**) and change of anatomy in white matter (**Figures 6G** and **7G**) are clearly observed. Therefore, the darkened fluorescence should be ascribed to the integration of subdural hematoma and anatomic change of white matter in the established acute spinal cord injury

model. Thus, this rapid and bright BMB technology may well be useful for monitoring the position and extent of intraoperative SCI in real time, which subsequently allows the use of remedial treatments for alleviating second injury and improving neurological function.

The BMB staining technology is considered to be safe for clinical use based on the following observations. Firstly, the BMB in both free and micellar formulation showed excellent cell biocompatibility in both PC-12 and L929 cells (**Figure S8**). Secondly, BMB was administered locally by epidural injection to diminish the side effects that may be caused by the distribution of BMB in other organs and tissues. This is also confirmed by the observation that no abnormal behaviors, intact motor and sensory functions were noted in the BMB-treated groups. Thirdly, BMB fluorescence disappeared at 24 h after epidural injection, indicating that BMB is readily metabolized from the spinal cord and most likely will not cause long-term toxicity. Therefore, the BMB has favorable biocompatibility and low toxicity in staining of spinal cord.

In conclusion, we introduced a BMB staining technology for rapid and effective imaging of the whole spinal cord via epidural administration, which may well significantly improve the safety of spine surgery. Moreover, the present work also demonstrated great potential of this technology in detection of intraoperative SCI.

## Conclusions

In this study, we demonstrated a nerve-highlighting fluorophore (*i.e.* BMB) in micellar form (BMB-m) can be used for rapid and effective imaging of the whole spinal cord in rabbit via epidural administration. The mechanism revealed that BMB is transported by the flow of CSF and binds to the peripheral white matter, resulting in rapid staining of the whole spinal cord. Furthermore, this technology also holds great potential for visually monitoring spinal cord integrity in real time and promptly identifying acute SCI during spine surgery. In general, our study has opened a new way for intraoperative imaging of CNS. A potential shortage of this imaging technology may be that the BMB is not a near-infrared probe. The development of this technology by using a newly designed fluorescent probe with long-wavelength emission [61, 62] should be one of the future directions.

## Abbreviations

SCI: spinal cord injury; BMB: (*E*, *E*)-1,4-bis(*p*-aminostyryl)-2-methoxy-benzene; CSF: cerebrospinal fluid; CNS: central nervous system;

MISS: minimally invasive spinal surgery; CT: computed tomography; MRI: magnetic resonance imaging; PET: positron emission tomography; IOM: Intraoperative electrophysiological monitoring; BMB-m: BMB-micelles; SEP: somatosensory evoked potentials; MEP: motor-evoked potentials; EMG: electromyography; CLSM: confocal laser scanning microscope; BBB: blood-brain barrier; FM: styrylpyridinium; FGS: fluorescence-guided surgery; MTT: 3-(4,5-dimethyl-thiazol-2-yl)-2,5-diphenyl tetrazolium bromide; DMSO: dimethyl sulfoxide; DLS: dynamic light scattering instrument; TEM: transmission electron microscopy; UV: ultraviolet; DMEM: Dulbecco's modified Eagle medium; FIS: fluorescence imaging system; LED: light emitting diode; CCD: charged-coupled device; PBS: phosphate buffered saline; RP-HPLC: reverse-phase high-performance liquid chromatography; ACN: acetonitrile; SC/A: fluorescence ratios of spinal cord to adipose; ANOVA: analysis of variance; SD: standard deviation; SC: spinal cord; WM: white matter; GM: grey matter; LF: ligamentum flavum; SP: spinous process

## Supplementary Material

Additional File 1:

Figures S1-S8. <http://www.thno.org/v07p1863s1.pdf>

Additional File 2:

Video S1. <http://www.thno.org/v07p1863s2.mp4>

## Acknowledgments

We thank W.K. Liu (Jilin University) for assistance with drawing schematic illustrations, H. Lian (Changchun Institute of Applied Chemistry) for help with cell culture, X.Y. Zhang (Jilin University) for assistance with operations in rabbits. This work was partially supported by the National Natural Science Foundation of China (grant numbers 51573184, 51390484, 51233004, 51321062).

## Competing Interests

The authors have declared that no competing interest exists.

## References

- Diaz E, Morales H. Spinal Cord Anatomy and Clinical Syndromes. *Semin Ultrasound CT MR*. 2016; 37: 360-71.
- Naderi S, Ture U, Pait TG. History of the spinal cord localization. *Neurosurg Focus*. 2004; 16: E15.
- Cramer DE, Maher PC, Pettigrew DB, Kuntz C 4th. Major neurologic deficit immediately after adult spinal surgery: incidence and etiology over 10 years at a single training institution. *J Spinal Disord Tech*. 2009; 22: 565-70.
- Pahys JM, Guille JT, D Andrea LP, Samdani AF, Beck J, Betz RR. Neurologic injury in the surgical treatment of idiopathic scoliosis: guidelines for assessment and management. *J Am Acad Orthop Surg*. 2009; 17: 426-34.
- Delank KS, Delank HW, KOnig DP, Popken F, FÜRderer S, Eysel P. Iatrogenic paraplegia in spinal surgery. *Arch Orthop Trauma Surg*. 2005; 125: 33-41.
- McDonald JW, Sadowsky C. Spinal-cord injury. *Lancet*. 2002; 359: 417-25.

- Alcanyis-Alberola M, Giner-Pascual M, Salinas-Huertas S, Gutiérrez-Delgado M. Iatrogenic spinal cord injury: an observational study. *Spinal Cord*. 2011; 49: 1188-92.
- Cho TA. Spinal cord functional anatomy. *Continuum (Minneapolis)*. 2015; 21: 13-35.
- Perez-Cruet MJ, Fessler RG, Perin NI. Review: complications of minimally invasive spinal surgery. *Neurosurgery*. 2002; 51(Suppl 5): S26-S36.
- Jaikumar S, Kim DH, Kam AC. History of minimally invasive spine surgery. *Neurosurgery*. 2002; 51(Suppl 5): S1-S14.
- Uribe JS, Vale FL, Dakwar E. Electromyographic monitoring and its anatomical implications in minimally invasive spine surgery. *Spine (Phila Pa 1976)*. 2010; 35(Suppl 26): S368-S374.
- Tali ET, Boyunaga O. The Spine and Spinal Cord in Children. In: Van Goethem JW, Den Hauwe LV, Parizel PM, ed. *Spinal Imaging: Diagnostic Imaging of the Spine and Spinal Cord*. Berlin, Heidelberg: Springer-Verlag Berlin Heidelberg; 2007: 43-83.
- Valladares-Otero A, Christenson B, Petersen BD. Radiologic Imaging of the Spine. In: Patel VV, Patel A, Harrop JS, Burger E, ed. *Spine Surgery Basics*. Berlin, Heidelberg: Springer-Verlag Berlin Heidelberg; 2014: 37-73.
- Glenn GR, Kuo LW, Chao YP, Lee CY, Helpem JA, Jensen JH. Mapping the Orientation of White Matter Fiber Bundles: A Comparative Study of Diffusion Tensor Imaging, Diffusional Kurtosis Imaging, and Diffusion Spectrum Imaging. *AJNR Am J Neuroradiol*. 2016; 37: 1216-22.
- Deletis V, Sala F. Intraoperative neurophysiological monitoring of the spinal cord during spinal cord and spine surgery: a review focus on the corticospinal tracts. *Clin Neurophysiol*. 2008; 119: 248-64.
- Malhotra NR, Shaffrey CI. Intraoperative electrophysiological monitoring in spine surgery. *Spine (Phila Pa 1976)*. 2010; 35: 2167-79.
- Schwartz DM, Auerbach JD, Dormans JP, Flynn J, Drummond DS, Bowe JA, et al. Neurophysiological detection of impending spinal cord injury during scoliosis surgery. *J Bone Joint Surg Am*. 2007; 89: 2440-9.
- Vercelli A, Repici M, Garbossa D, Grimaldi A. Recent techniques for tracing pathways in the central nervous system of developing and adult mammals. *Brain Res Bull*. 2000; 51: 11-28.
- Lanciego JL, Wouterlood FG. A half century of experimental neuroanatomical tracing. *J Chem Neuroanat*. 2011; 42: 157-83.
- Sekiguchi KJ, Shekhtmeyster P, Merten K, Arena A, Cook D, Hoffman E, et al. Imaging large-scale cellular activity in spinal cord of freely behaving mice. *Nat Commun*. 2016; 7: 11450.
- Livet J, Weissman TA, Kang H, Draft RW, Lu J, Bennis RA, et al. Transgenic strategies for combinatorial expression of fluorescent proteins in the nervous system. *Nature*. 2007; 450: 56-62.
- Tsien RY. Nobel lecture: constructing and exploiting the fluorescent protein paintbox. *Integr Biol (Camb)*. 2010; 2: 77-93.
- Shcherbo D, Merzlyak EM, Chepurnykh TV, Fradkov AF, Ermakova GV, Solovieva EA, et al. Bright far-red fluorescent protein for whole-body imaging. *Nat Methods*. 2007; 4: 741-6.
- Shcherbakova DM, Balaban M, Emelyanov AV, Brenowitz M, Guo P, Verkhusha VV. Bright monomeric near-infrared fluorescent proteins as tags and biosensors for multiscale imaging. *Nat Commun*. 2016; 7: 12405.
- Whitney MA, Crisp JL, Nguyen LT, Friedman B, Gross LA, Steinbach P, et al. Fluorescent peptides highlight peripheral nerves during surgery in mice. *Nat Biotechnol*. 2011; 29: 352-6.
- Gibbs-Strauss SL, Vooght C, Fish KM, Nasr KA, Siclován TM, Barnhardt NE, et al. Molecular imaging agents specific for the annulus fibrosus of the intervertebral disk. *Mol Imaging*. 2010; 9: 128-40.
- Massaad CA, Zhang G, Pillai L, Azhdarinia A, Liu W, Sheikh KA. Fluorescently-tagged anti-ganglioside antibody selectively identifies peripheral nerve in living animals. *Sci Rep*. 2015; 5: 15766.
- van Dam GM, Themelis G, Crane LM, Harlaar NJ, Pleijhuis RG, Kelder W, et al. Intraoperative tumor-specific fluorescence imaging in ovarian cancer by folate receptor- $\alpha$  targeting: first in-human results. *Nat Med*. 2011; 17: 1315-9.
- Stummer W, Pichlmeier U, Meinel T, Wiestler OD, Zanella F, Reulen HJ, et al. Fluorescence-guided surgery with 5-aminolevulinic acid for resection of malignant glioma: a randomised controlled multicentre phase III trial. *Lancet Oncol*. 2006; 7: 392-401.
- Craig SE, Wright J, Sloan AE, Brady-Kalnay SM. Fluorescent-Guided Surgical Resection of Glioma with Targeted Molecular Imaging Agents: A Literature Review. *World Neurosurg*. 2016; 90: 154-63.
- Chi C, Du Y, Ye J, Kou D, Qiu J, Wang J, et al. Intraoperative imaging-guided cancer surgery: from current fluorescence molecular imaging methods to future multi-modality imaging technology. *Theranostics*. 2014; 4: 1072-84.
- Zheng J, Muhanna N, De Souza R, Wada H, Chan H, Akens MK, et al. A multimodal nano agent for image-guided cancer surgery. *Biomaterials*. 2015; 67: 160-8.
- Wada H, Hyun H, Vargas C, Gravier J, Park G, Gioux S, et al. Pancreas-targeted NIR fluorophores for dual-channel image-guided abdominal surgery. *Theranostics*. 2015; 5: 1-11.
- Park MH, Hyun H, Ashitate Y, Wada H, Park G, Lee JH, et al. Prototype nerve-specific near-infrared fluorophores. *Theranostics*. 2014; 4: 823-33.
- Rigg JR, Jamrozik K, Myles PS, Silbert BS, Peyton PJ, Parsons RW, et al. Epidural anaesthesia and analgesia and outcome of major surgery: a randomised trial. *Lancet*. 2002; 359: 1276-82.

36. Kreiner DS, Hwang SW, Easa JE, Resnick DK, Baisden JL, Bess S, et al. An evidence-based clinical guideline for the diagnosis and treatment of lumbar disc herniation with radiculopathy. *Spine J*. 2014; 14: 180-91.
37. Wu CL, Cohen SR, Richman JM, Rowlingson AJ, Courpas GE, Cheung K, et al. Efficacy of postoperative patient-controlled and continuous infusion epidural analgesia versus intravenous patient-controlled analgesia with opioids: a meta-analysis. *Anesthesiology*. 2005; 103:1079-88.
38. Stankoff B, Wang Y, Bottlaender M, Aigrot MS, Dolle F, Wu C, et al. Imaging of CNS myelin by positron-emission tomography. *Proc Natl Acad Sci U S A*. 2006; 103: 9304-9.
39. Wu C, Wei J, Tian D, Feng Y, Miller RH, Wang Y. Molecular probes for imaging myelinated white matter in CNS. *J Med Chem*. 2008; 51: 6682-8.
40. Gibbs-Strauss SL, Nasr KA, Fish KM, Khullar O, Ashitate Y, Siclovan TM, et al. Nerve-highlighting fluorescent contrast agents for image-guided surgery. *Mol Imaging*. 2011; 10: 91-101.
41. Hackman KM, Doddapaneni BS, Barth CW, Wierzbicki IH, Alani AW, Gibbs SL. Polymeric Micelles as Carriers for Nerve-Highlighting Fluorescent Probe Delivery. *Mol Pharm*. 2015; 12: 4386-94.
42. National Research Council (US) Committee for the Update of the Guide for the Care and Use of Laboratory Animals. *Guide for the Care and Use of Laboratory Animals*, 8th ed. Washington (DC): National Academies Press (US); 2011.
43. Rivlin AS, Tator CH. Effect of duration of acute spinal cord compression in a new acute cord injury model in the rat. *Surg Neurol*. 1978; 10: 38-43.
44. Allen, A.R. Surgery of experimental lesion of spinal cord equivalent to crush injury of fracture dislocation of spinal column: a preliminary report. *JAMA*. 1911; 57: 878-80.
45. Allen, A.R. Remarks on the histopathological changes in the spinal cord due to impact. An experimental study. *Journal of Nervous and Mental Disease*. 1914; 41: 141-7.
46. Shen DD, Artru AA, Adkison KK. Principles and applicability of CSF sampling for the assessment of CNS drug delivery and pharmacodynamics. *Adv Drug Deliv Rev*. 2004; 56: 1825-57.
47. Clement R, Malinovsky JM, Le Corre P, Dollo G, Chevanne F, Le Verge R. Cerebrospinal fluid bioavailability and pharmacokinetics of bupivacaine and lidocaine after intrathecal and epidural administrations in rabbits using microdialysis. *J Pharmacol Exp Ther*. 1999; 289: 1015-21.
48. Miyajima M, Arai H. Evaluation of the Production and Absorption of Cerebrospinal Fluid. *Neurol Med Chir (Tokyo)*. 2015; 55: 647-56.
49. Matsumae M, Sato O, Hirayama A, Hayashi N, Takizawa K, Atsumi H, et al. Research into the Physiology of Cerebrospinal Fluid Reaches a New Horizon: Intimate Exchange between Cerebrospinal Fluid and Interstitial Fluid May Contribute to Maintenance of Homeostasis in the Central Nervous System. *Neurol Med Chir (Tokyo)*. 2016; 56: 416-41.
50. Weller RO. Microscopic morphology and histology of the human meninges. *Morphologie*. 2005; 89: 22-34.
51. Nicholas DS, Weller RO. The fine anatomy of the human spinal meninges. A light and scanning electron microscopy study. *J Neurosurg*. 1988; 69: 276-82.
52. Bernards CM, Hill HF. Physical and chemical properties of drug molecules governing their diffusion through the spinal meninges. *Anesthesiology*. 1992; 77: 750-6.
53. Bernards CM, Hill HF. Morphine and alfentanil permeability through the spinal dura, arachnoid, and pia mater of dogs and monkeys. *Anesthesiology*. 1990; 73: 1214-9.
54. Reina MA, Prats-Galino A, Sola RG, Puigdemívol-Sánchez A, Arriazu Navarro R, De Andrés JA. [Structure of the arachnoid layer of the human spinal meninges: a barrier that regulates dural sac permeability]. *Rev Esp Anestesiol Reanim*. 2010; 57: 486-92.
55. Moore RA, Bullingham RE, McQuay HJ, Hand CW, Aspel JB, Allen MC, et al. Dural permeability to narcotics: in vitro determination and application to extradural administration. *Br J Anaesth*. 1982; 54: 1117-28.
56. Clement R, Malinovsky JM, Hildgen P, Dollo G, Estebe JP, Chevanne F, et al. Spinal disposition and meningeal permeability of local anesthetics. *Pharm Res*. 2004; 21: 706-16.
57. Di Chiro G. Movement of the Cerebrospinal Fluid in Human Beings. *Nature*. 1964; 204: 290-1.
58. Di Chiro G. Observations on the circulation of the cerebrospinal fluid. *Acta Radiol Diagn (Stockh)*. 1966; 5: 988-1002.
59. Greitz D, Hannerz J. A proposed model of cerebrospinal fluid circulation: observations with radionuclide cisternography. *AJNR Am J Neuroradiol*. 1996; 17: 431-8.
60. Oreskovic D, Klarica M. A new look at cerebrospinal fluid movement. *Fluids Barriers CNS*. 2014; 11: 16.
61. Siclovan TM, Zhang R, Cotero V, Bajaj A, Dylov DV, Yazdanfar S, et al. Fluorescence Phenomena in Nerve-Labeling Styryl-Type Dyes. *J Photochem Photobiol A Chem*. 2016; 316: 104-16.
62. Barth CW, Gibbs SL. Direct Administration of Nerve-Specific Contrast to Improve Nerve Sparing Radical Prostatectomy. *Theranostics*. 2017; 7: 573-93.